# 9 Particle physics with CMS

E. Alagöz, C. Amsler, V. Chiochia, Hp. Meyer, C. Regenfus, P. Robmann, J. Rochet, T. Rommerskirchen, A. Schmidt[5], T. Speer[6], S. Steiner, D. Tsirigkas, and L. Wilke

*In collaboration with:* ETH - Zürich, Paul Scherrer Institut (PSI) and the CMS Collaboration

We have been involved in the design, construction and test of the CMS barrel pixel detector since many years. In particular, we have conducted various performance tests on beams at CERN (1). The position resolution, the Lorentz angle and the detection efficiency were determined on highly irradiated pixel prototypes. We also deliver the offline software for reconstructing and simulating hits and tracks in the CMS pixel (and strip) detectors, and contribute to the data quality monitoring and alignment codes. The group is furthermore active in the development of algorithms required to efficiently tag $B$-hadrons, using the pixel vertex detector. The year 2007 and early 2008 were dedicated to the completion of the pixel hardware and to the preparation of the software for data taking and data analysis.

The pixel detector is currently being completed in our institute and at PSI. The institute's workshop manufactured the two detector support structure half-shells for the pixel detector. Figure 9.1 shows the third layer of the final support structure with the mounted pixel detector modules. The production of the final supply tube half-shells is also completed. The electrical power and control lines, the optical signal lines and the cooling fluid are transferred across the supply tubes to the pixel detector. Figure 9.2 shows a supply tube half-shell. The structure consists of thin stainless steel tubes and inner and outer aluminium flanges. The tubes supply the detector with the cooling fluid. The gaps are filled with foam. The power and slow control leads are embedded in the supply tube body. Our electronics workshop manufactured all parts and the detector front end control system. The system consists of four communication and control unit boards, each controling a quarter of the detector with eight barrel readout sectors.

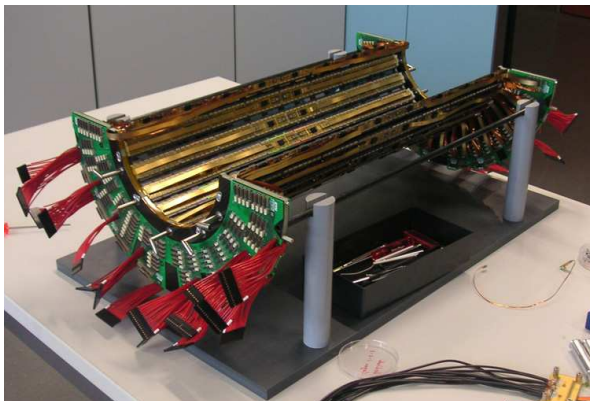

**Figure 9.1: Support structure of the third (outer) layer with pixel detector modules.**

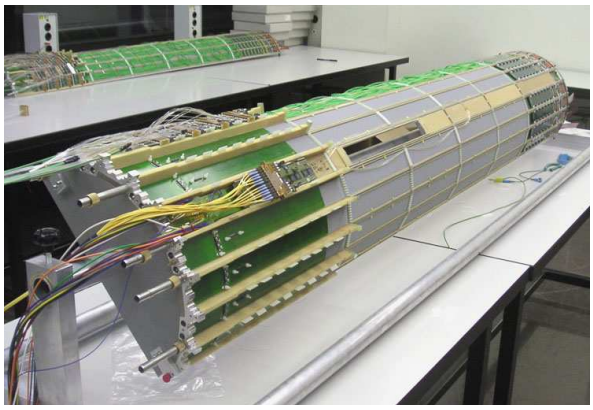

**Figure 9.2: Supply tube half-shell during the installation of the electronics boards, the optohybrids and optical fibres. A fully equipped half-shell can be seen in the back.**

[5]Since 1 September 2007
[6]Until 31 August 2007, now at Brown University

A final pixel sensor test had been performed at CERN in autumn 2006. We used a beam telescope with four pixel sensors, two in front and two behind the pixel sensors under test. The 52 $\times$ 80 pixel device had the final CMS dimensions 150 $\times$ 100 $\mu$m$^2$ with a thickness of 285 $\mu$m. They were bump-bonded to final CMS pixel readout chips. A PIN diode (3 $\times$ 6 $\mathrm{mm}^2$) was used as a trigger. Irradiated sensors were kept at $-10^{\circ}\mathrm{C}$ in a cooling box with two Peltier elements. The experimental setup was placed in a Helmholtz superconductor magnet, providing a transverse field of 3T, and was exposed to a 150 GeV $\pi^-$ beam. Data were taken with and without magnetic field for several bias voltages. The purpose of the test was to compare real data with the predictions obtained from our previous runs which used pixels of different dimensions and a magnetic field parallel to the incident pions (2).

The analysis of these data was performed in 2007, involving in particular a careful alignment procedure of the detectors to obtain the best possible resolution in the measurement of the directions of the incident pions. The charge collection in the test module is shown in Fig. 9.3 for several irradiated and unirradiated samples at 200 V bias. One observes a decrease of the collected charge for higher irradiation fluences. The collected charge is reduced to 46 % for fluences of $6.2 \times 10^{14}\mathrm{n_{eq}cm^{-2}}$ which will be absorbed by the CMS pixel sensors after two years of run at full LHC luminosity. The collected charge is reduced by defects due to radiation damage, which work as charge trapping centers. The charge loss is larger in the magnetic field since the drift length of the electrons increases due to Lorentz deflection. Increasing the bias voltage can recover some of the lost charge (Fig. 9.4), however at the expense of a reduced drift path, and hence reduced charge sharing, which in turn decreases the accuracy of the position resolution.

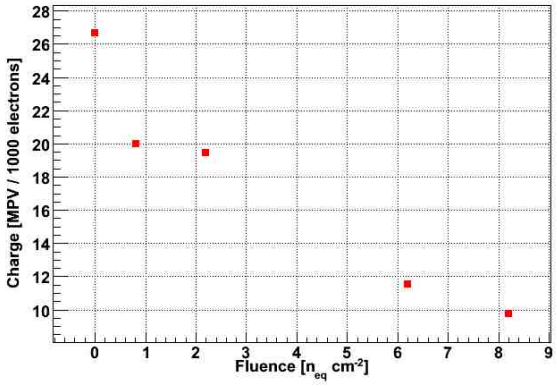


**Figure 9.3: Charge collection efficiency for unirradiated and irradiated pixel sensors at 200 V, as a function of fluence.**

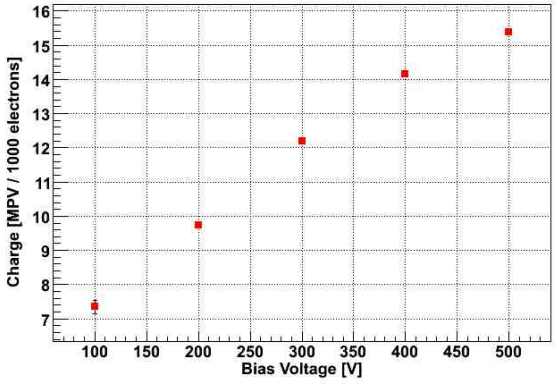


**Figure 9.4: Charge collection efficiency for heavily irradiated pixel sensors ($8\times10^{14}\mathrm{n}_{eq}\mathrm{cm}^{-2}$) as a function of bias voltage.**

Several new features have been implemented in the pixel software, such as a precise description of the material thickness, especially in the complicated regions of the pixel end-caps. Online pixel calibration runs will provide in real time gain response functions for each channel. The size of the calibration tables was reduced substantially to comply with the memory requirements of the CMS reconstruction programs. Detailed simulations have shown that such reductions will have negligible effects on position resolution and $b$-tagging efficiency.

The alignment of the tracking detectors is a major challenge in the early phase of the experiment. Tracker misalignment (e.g. due to imprecise mounting of sensors or moving structures due to thermal and magnetic field effects) will impair the hit, track and vertex reconstructions, and will decrease the $b$-tagging efficiency. We have developed a simple algorithm relying on the presence of a secondary vertex and taking the separation between primary and secondary vertex as discriminator. This algorithm does not require a dedicated calibration, is simple and robust enough to be used in the early stage of the experiment. However, the secondary vertex finding efficiency is only 55%. The detector alignment procedure will quickly improve as soon as data from resonances such as $J/\psi$ and gauge bosons become available.

We made important contributions to track reconstruction and $b$-flavour tagging in fast simulation and are responsible for the interface and maintenance of the $b$-tagging algorithms in a fast simulation software. Figure 9.5 demonstrates the impressive agreement in terms of $b$-tagging efficiency and charm mistagging rate, comparing fast and full detector simulations.

In the pixel sensors the electrons produced by ionizing particles experience a Lorentz force and drift perpendicular to the 4T magnetic field and the bias electric field. This leads to a shift in the measured coordinates which can be up to 120 $\mu$m. This shift has been measured for un-irradiated sensors. However, during LHC operation the bias voltage will be increased to compensate for radiation damage (see Fig. 9.3) and hence the Lorentz deflection angle will decrease. Furthermore, each detector module will have a different evolution due to non uniform irradiation. Therefore the Lorentz drift needs to be monitored directly from data. Figure 9.6 shows a simulation of the coordinate shift $d$ as a function of depth $z$ in the pixel sensor at which the charge was produced. The average shift can be determined for a given depth with a large number of well-measured tracks (Fig. 9.7). The slope is the tangent of the Lorentz angle. Such a measurement is done independently for the eight module rings in the three detector layers. Studies for different input values of the Lorentz angle in the detector simulation were performed, as well as studies on the influence of misalignment.

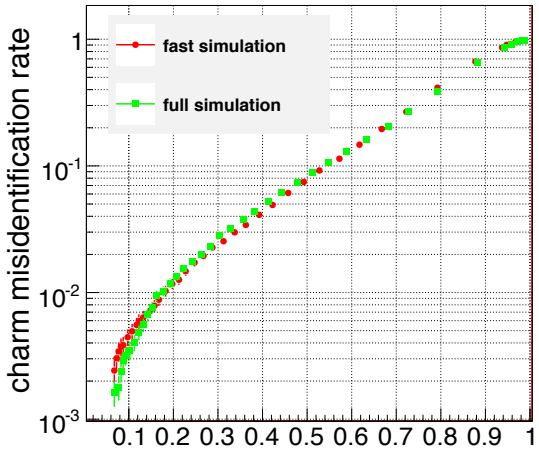


**Figure 9.5: Charm mistagging rate vs. b-tagging efficiency in fast and full detector simulations.**

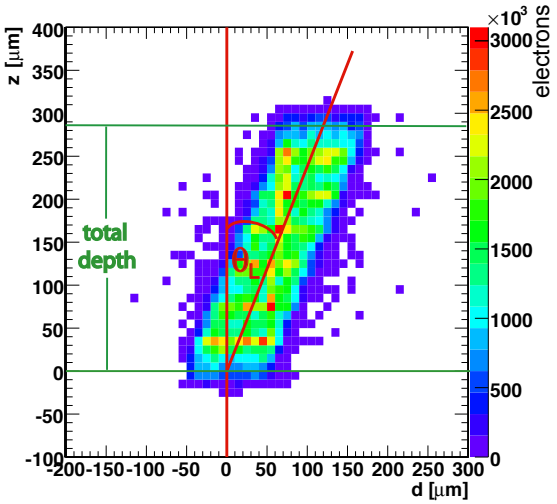


**Figure 9.6: Depth z at which the drift electrons were produced vs. readout coordinate d (simulation for muon tracks crossing the pixel detector at a pseudo-rapidity $\eta$=2).**

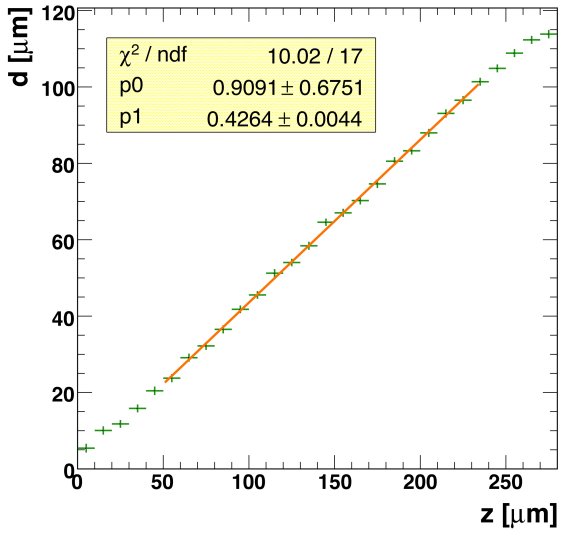


**Figure 9.7: Average drift of electrons d as a function of the production depth z in the silicon sensor bulk. The solid line shows the fit.**

During the first two years of LHC operation we will concentrate on $b$-physics issues which can be performed at low luminosity. In particular, we will study the decay $B_s^0 \rightarrow (J/\psi)\phi \rightarrow \mu^+\mu^- K^+K^-$ and measure the lifetimes of the CP-eigenstates $B_s^H$ and $B_s^L$. This channel has been chosen as a benchmark channel by the CMS collaboration (3). A dedicated trigger for $B$-mesons decaying into two muons via a $J/\psi$ intermediate states was developed, based on the long time of flight of the B-mesons. The secondary vertex of the two muons is reconstructed applying quality cuts on the decay length significance, and on the invariant mass of the two muons. We developed an analysis strategy for the first 100 pb$^{-1}$ expected at the LHC in 2009. The first step is to measure the detector performance using the well known channel $B_d \rightarrow J/\psi K^* \rightarrow \mu^+\mu^- K^+\pi-$. This channel has very similar properties as the $B_s$-channel and all parameters have been measured to high precision by BaBar and Belle.

We are also preparing a search for supersymmetry which might be observed early at the LHC. A prominent signature is the presence of multiple jets + high missing transverse energy (MET) + two or more $b$-jets. The potential background stems from $t\bar{t}$, $W$ + jets, $Z^0$ + jets and QCD events. An interesting process is the light Higgs-boson $h$-decay in SUSY processes, $\tilde{q} \rightarrow \tilde{\chi}_2^0 q, \tilde{\chi}_2^0 \rightarrow \tilde{\chi}_1^0 h, h \rightarrow b\bar{b}$, where $\chi_1^0$ and $\chi_2^0$ are neutralinos (4). The former is stable in $R$-parity conserving SUSY and therefore leads to a large missing energy.

We have simulated this channel by first requiring from the online trigger and at least 3 jets. In the offline analysis we require more than 5 energetic ($>$ 30 GeV) jets and a missing transverse energy of at least 240 GeV. A relevant parameter is the average direction of particles associated with a high energy jet, in particular its azimuthal angle $\phi$ transverse to the incident beam directions. The angles $\Delta\phi$ between the direction of the missing energy and those of the two most energetic jets is required to be at least 12°. From measurements of the impact parameters we also keep events with two $b$-jets. The result is shown in Fig. 9.8 which displays the predicted $b\bar{b}$ invariant mass distribution for an integrated luminosity of 100 pb$^{-1}$, after all cuts. The $h \rightarrow b\bar{b}$ signal (8 $\pm$ 1 events) shown by the red histogram is only a small contribution to all SUSY events. The main background stems from $t\bar{t}$ and QCD events, while contributions from $W$- and $Z^0$-decays associated with jet production are negligible.

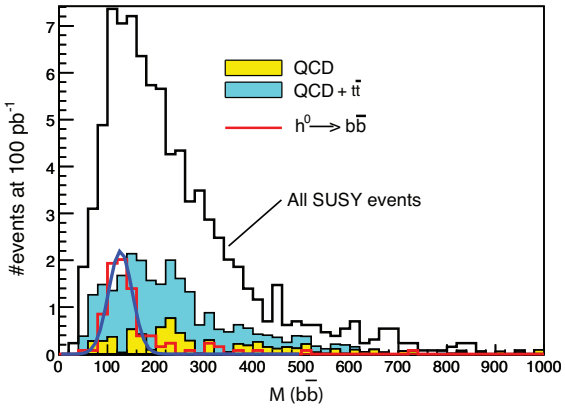


**Figure 9.8: Invariant mass of two b-tagged jets after all selection cuts for SUSY and for background events (simulation). The red curve shows the fit to $h \rightarrow b\bar{b}$.**

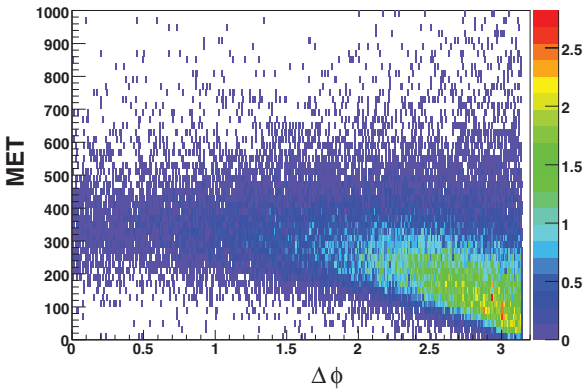


**Figure 9.9: Missing transverse energy (MET) vs. $\Delta\phi$ for the LM1 point in the mSUGRA parameter space.**

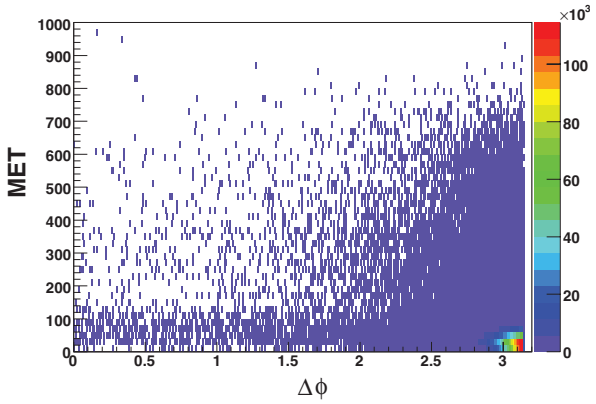


**Figure 9.10: MET vs. $\Delta\phi$ for QCD events ($120 < p_T < 1000$ GeV/c).**

For an integrated luminosity of 100 pb$^{-1}$ the significance of the signal peak ($43 \pm 2$ events) is about $8\sigma$.

Figures 9.9 and 9.10 show the dependence of MET on $\Delta\phi$, the angle between the two most energetic jets, for SUSY and QCD events. It appears that, for large missing energies, the two most energetic jets are emitted in opposite directions (large $\Delta\phi$) for QCD events, while for the popular LM1-point of SUSY/mSUGRA they are more isotropically distributed. For the latter there is also a strong correlation between MET and $\Delta\phi$ (green/yellow region in Fig. 9.9). These features can be used to further decrease the QCD background.

The installation of the pixel detector in CMS is scheduled for May 2008. However, pixel readout tests have already been made in the CMS experimental area with a panel of the endcap pixel detector. Runs with several readout thresholds were recorded for the first time in March 2008 on the CERN TIER 0 storage, using the global CMS data acquisition, and were analyzed with the pixel data quality monitoring software. Results were in line with expectations. Our software codes will be deployed for the global run with the 3.8 T magnetic field scheduled in June 2008, just before LHC is expected to deliver its first beams.

[1] Y. Allkofer *et al.*. Nucl. Instrum. Meth. in Phys. Research **A 584** (2008) 25.

[2] A. Dorokhov *et al.*, Nucl. Instr. Meth. in Phys. Research **A 530** (2004) 71;
A. Dorokhov *et al.*, Nucl. Instr. Meth. in Phys. Research **A 560** (2006) 112;
V. Chiochia *et al.*, IEEE Trans. Nucl. Sci. **52** (2005) 1067.

[3] The CMS collaboration, "CMS Physics Technical Design Report Volume II:
Physics Performance", CERN/LHCC 2006-021, CMS TDR 8.2, 2006.

[4] F. Moortgat, P. Olbrechts, L. Pape and A. Romeyer, CMS Note 2006/090.